A Rayleigh wave back-projection method applied to the 2011 Tohoku earthquake

Daniel Roten, Hiroe Miyake, and Kazuki Koketsu (2012), *GRL*

Earthquake of the Week - 27 January 2012

Roten, D., H. Miyake, and K. Koketsu (2012), A Rayleigh wave back-projection method applied to the 2011 Tohoku earthquake, *Geophys. Res. Lett.*, 39, L02302, doi:10.1029/2011GL050183.

Motivation and Summary

Motivation and Summary

Region of maximum slip in recent source inversions of 11 March, 2011

M_w 9.1 EQ strongly data-dependent:

- Near trench [e.g. Lay et al., 2011; Pollitz et al., 2011]
- Near JMA hypocenter [e.g. Ammon et al., 2011; Simons et al., 2011]
- Down-dip of JMA hypocenter beneath coastline [e.g. Meng et al., 2011]

Up-dip extent of rupture overall difficult to assess [e.g. Lay et al., 2011]

Motivation and Summary

Region of maximum slip in recent source inversions of 11 March, 2011

M_w 9.1 EQ strongly data-dependent:

- Near trench [e.g. Lay et al., 2011; Pollitz et al., 2011]
- Near JMA hypocenter [e.g. Ammon et al., 2011; Simons et al., 2011]
- Down-dip of JMA hypocenter beneath coastline [e.g. Meng et al., 2011]

Up-dip extent of rupture overall difficult to assess [e.g. Lay et al., 2011]

Authors suggest frequency-dependent radiation as potential explanation [e.g. Koper et al., 2011]

Motivation and Summary

Region of maximum slip in recent source inversions of 11 March, 2011

M_w 9.1 EQ strongly data-dependent:

- Near trench [e.g. Lay et al., 2011; Pollitz et al., 2011]
- Near JMA hypocenter [e.g. Ammon et al., 2011; Simons et al., 2011]
- Down-dip of JMA hypocenter beneath coastline [e.g. Meng et al., 2011]

Up-dip extent of rupture overall difficult to assess [e.g. Lay et al., 2011]

Authors suggest frequency-dependent radiation as potential explanation [e.g. Koper et al., 2011]

Employ multi-frequency (T=13-100 s) surface-wave back projection in order to assess this effect

Methods: Back projection

Methods: Back projection

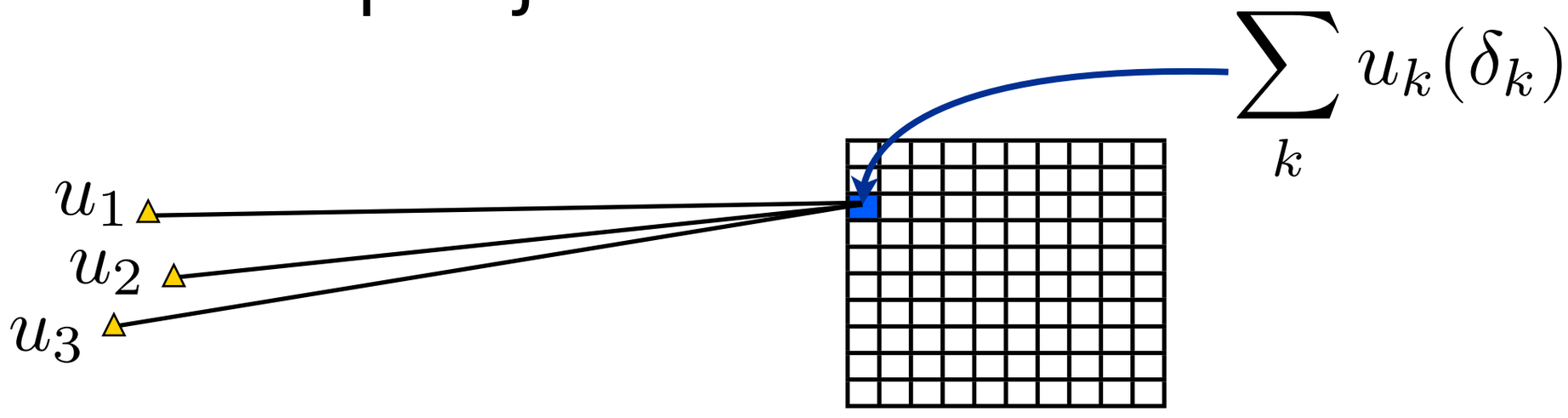

Given grid of potential source locations, identification by waveform stacking and migration to predicted travel time of chosen phase

Want: highest amplitude phase, well-separated

Methods: Back projection

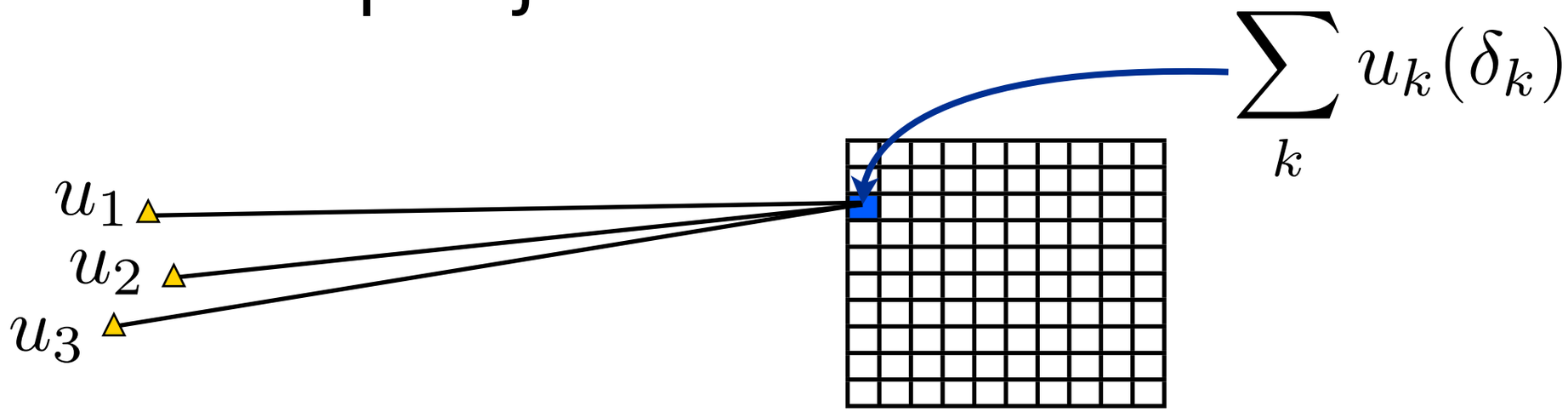

Given grid of potential source locations, identification by waveform stacking and migration to predicted travel time of chosen phase

Want: highest amplitude phase, well-separated

P arrival used successfully for teleseismic body-wave BP, but local to regional distances difficult:

Local distance: little separation between P and stronger S

Regional distance: (>150km) S_n before direct S_g, followed by strong L_g

Methods: Back projection

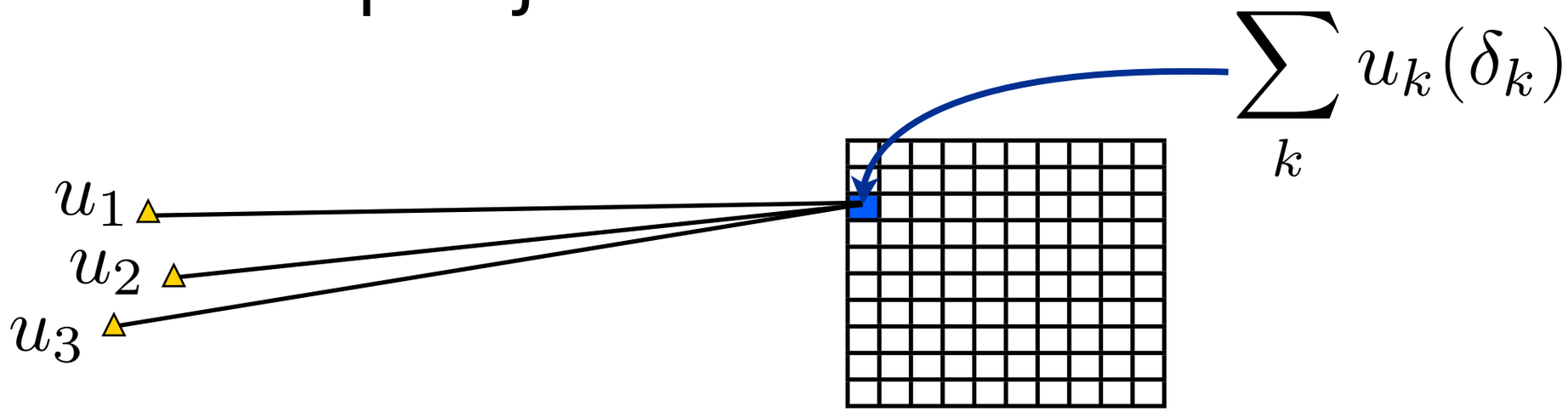

Given grid of potential source locations, identification by waveform stacking and migration to predicted travel time of chosen phase

Want: highest amplitude phase, well-separated

P arrival used successfully for teleseismic body-wave BP, but local to regional distances difficult:

Local distance: little separation between P and stronger S

Regional distance: (>150km) S_n before direct S_g, followed by strong L_g

Authors use Rayleigh wave BP from K-NET and KiK-net recordings, as these phases are both *strong* and *dispersive*

Methods: Waveform processing

Methods: Waveform processing

Authors use a continuous wavelet transform in order to isolate energy at the period of interest:

$$wt_k(s,\tau) = \frac{1}{\sqrt{s}} \int_{-\infty}^{+\infty} u_k(t)\psi^* \left(\frac{t-\tau}{s} \right) \; dt$$

Methods: Waveform processing

Authors use a continuous wavelet transform in order to isolate energy at the period of interest:

$$wt_k(s,\tau) = \frac{1}{\sqrt{s}} \int_{-\infty}^{+\infty} u_k(t) \psi^* \left(\frac{t-\tau}{s} \right) \, dt$$

where $$\psi_B(t) = \sqrt{f_b} \left[\mathrm{sinc} \left(\frac{f_b t}{p} \right) \right]^p \exp\{2\pi i f_c t\}$$

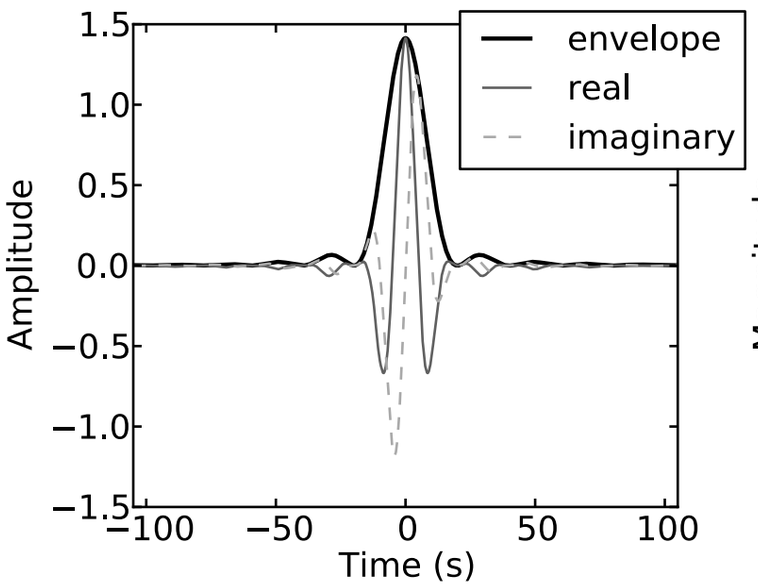

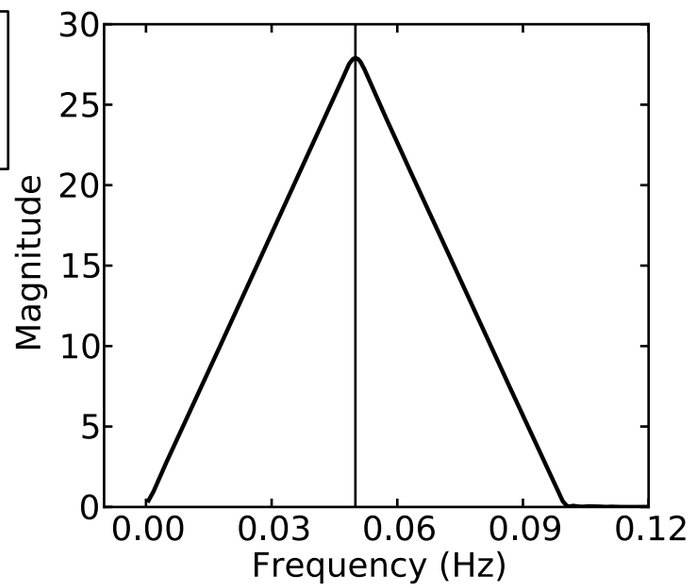

f_b bandwidth

f_c center

Chose 1 Hz center in mother wavelet - scale becomes period

Methods: Waveform processing

Authors use a continuous wavelet transform in order to isolate energy at the period of interest:

Synthetic (FD) example for vertical component waveforms of M_w 7.3 foreshock (T=13s)

Rayleigh waves clearly visible as strongest phases in CWT envelopes

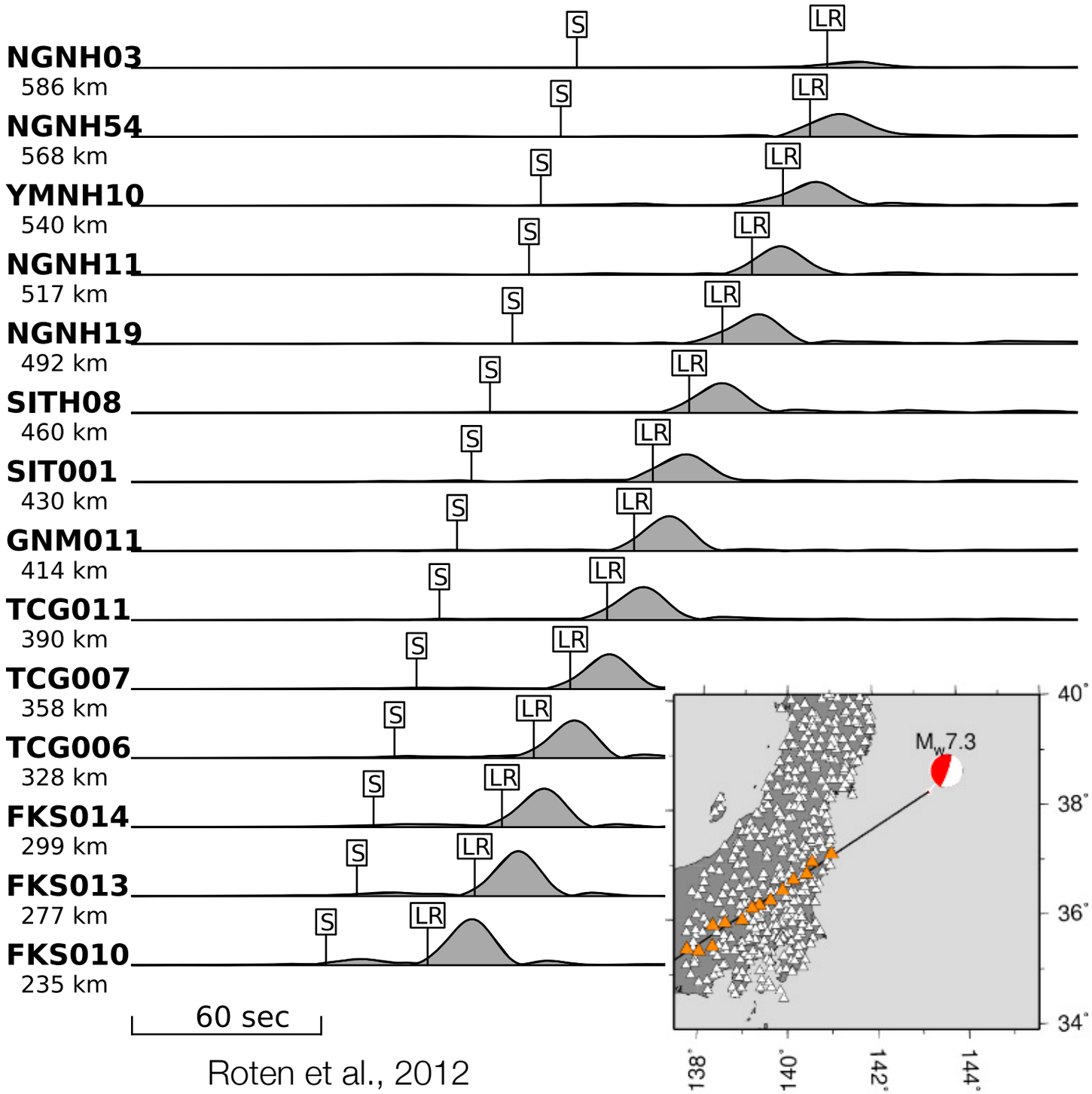

Roten et al., 2012

Methods: Back projection (again)

Methods: Back projection (again)

$$S_m(s,\tau) = \left| \sum_{k=1}^{N} wt_k(s, \tau + \delta_{m,k}) \; w_{m,k} \; p_{m,k} \right|^2$$

Authors take square modulus of migrated, *weighted*, stacked waveforms

s	period
τ	source time
m	source index
k	station index

Methods: Back projection (again)

$$S_m(s,\tau) = \left| \sum_{k=1}^{N} wt_k(s, \tau + \delta_{m,k}) \; w_{m,k} \; p_{m,k} \right|^2$$

Authors take square modulus of migrated, *weighted*, stacked waveforms

s	period
τ	source time
m	source index
k	station index

$w_{m,k}$ source-station azimuth weighting

$$\frac{1}{w_{m,k}} = \sum_{i=1}^{N} 1 - \frac{|\theta_{m,i} - \theta_{m,k}|}{\Delta\theta}$$

Methods: Back projection (again)

$$S_m(s,\tau) = \left| \sum_{k=1}^{N} wt_k(s, \tau + \delta_{m,k}) \; w_{m,k} \; p_{m,k} \right|^2$$

Authors take square modulus of migrated, *weighted*, stacked waveforms

s	period
τ	source time
m	source index
k	station index

$w_{m,k}$ source-station azimuth weighting

$$\frac{1}{w_{m,k}} = \sum_{i=1}^{N} 1 - \frac{|\theta_{m,i} - \theta_{m,k}|}{\Delta\theta}$$

$p_{m,k}$ source-station distance weighting

zero for distances less than 100 km

Methods: Back projection (again)

$$S_m(s,\tau) = \left| \sum_{k=1}^{N} wt_k(s, \tau + \delta_{m,k})\ w_{m,k}\ p_{m,k} \right|^2$$

Authors take square modulus of migrated, *weighted*, stacked waveforms

s	period
τ	source time
m	source index
k	station index

$w_{m,k}$ source-station azimuth weighting

$$\frac{1}{w_{m,k}} = \sum_{i=1}^{N} 1 - \frac{|\theta_{m,i} - \theta_{m,k}|}{\Delta\theta}$$

$p_{m,k}$ source-station distance weighting

zero for distances less than 100 km

$\delta_{m,k}$ Predicted travel time from group-velocity dispersion map

Methods: Back projection (again)

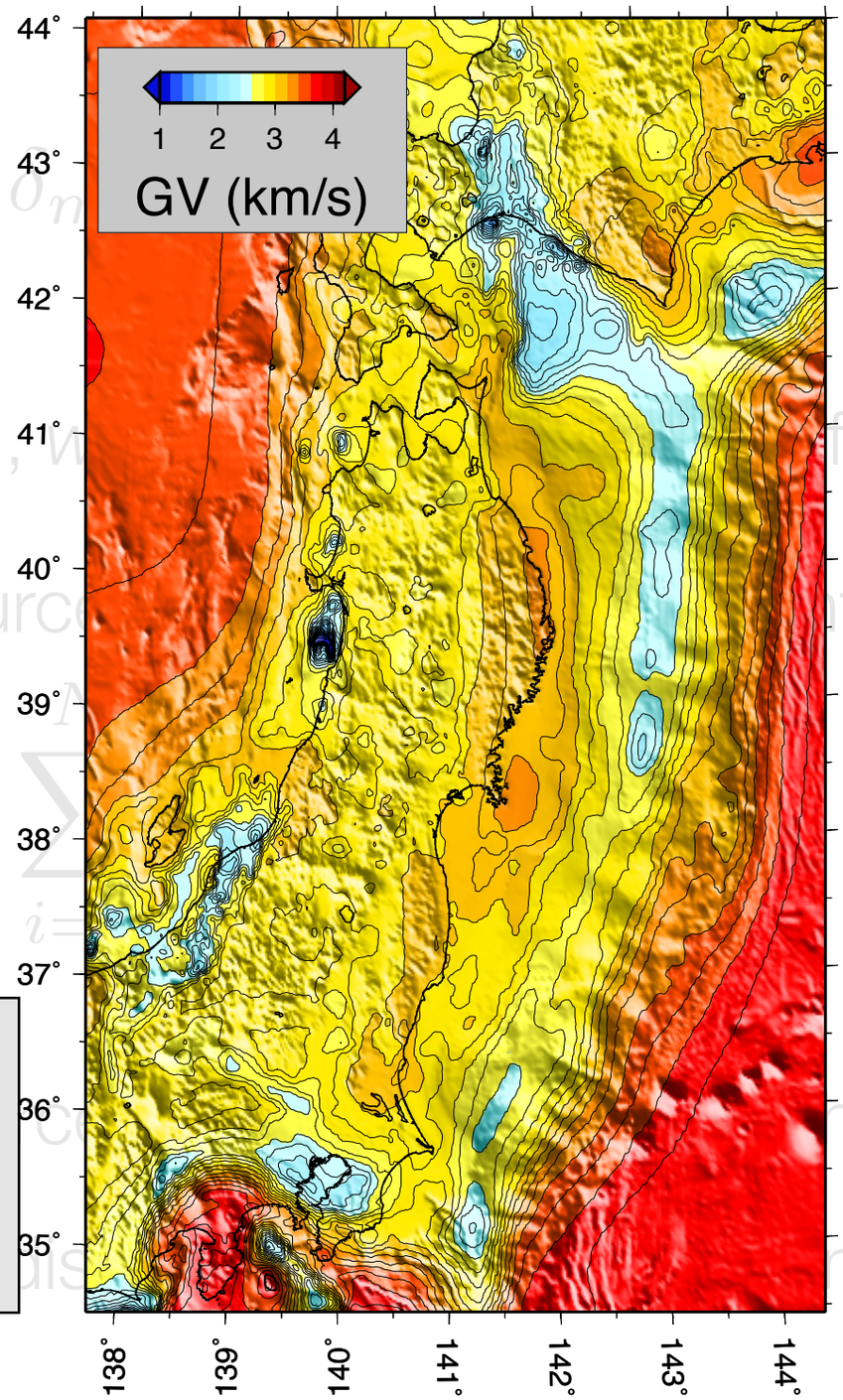

Right: Fundamental-mode Rayleigh wave group velocities derived from the Japan Integrated Velocity Structure Model (JIVSM) [Koketsu et al., 2008] - here shown for T=20s.

$\delta_{m,k}$ Predicted travel time from group-velocity dispersion map

Methods: Synthetic validation

FD simulation of Mw 7.3 foreshock as a point source in the Japan Integrated Velocity Structure Model [Koketsu et al., 2008]

Stack maximum at zero time and true location

Ghost peaks migrate from ESE to WNW

At right: BP of M_w 7.3 foreshock radial-component synthetics (T=20s) using same 384 stations as in later study of M_w 9.1 mainshock

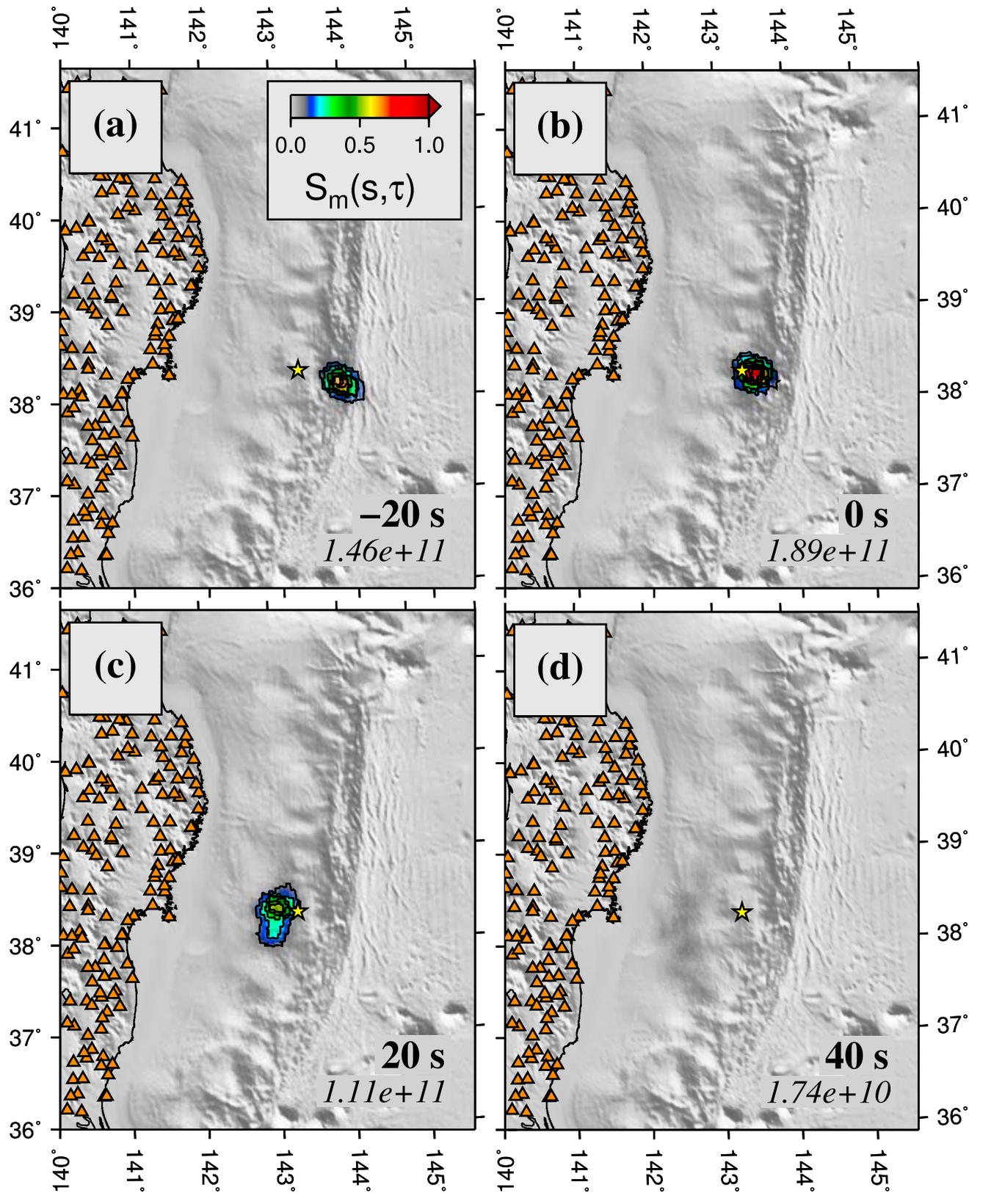

Methods: Synthetic validation

FD simulation of Mw 7.3 foreshock as a point source in the Japan Integrated Velocity Structure Model [Koketsu et al., 2008]

Stack maximum at zero time and true location

Ghost peaks migrate from ESE to WNW

At right: *T*=20s array response function estimate for the 384 K-NET / KiK-net stations used in mainshock BP.

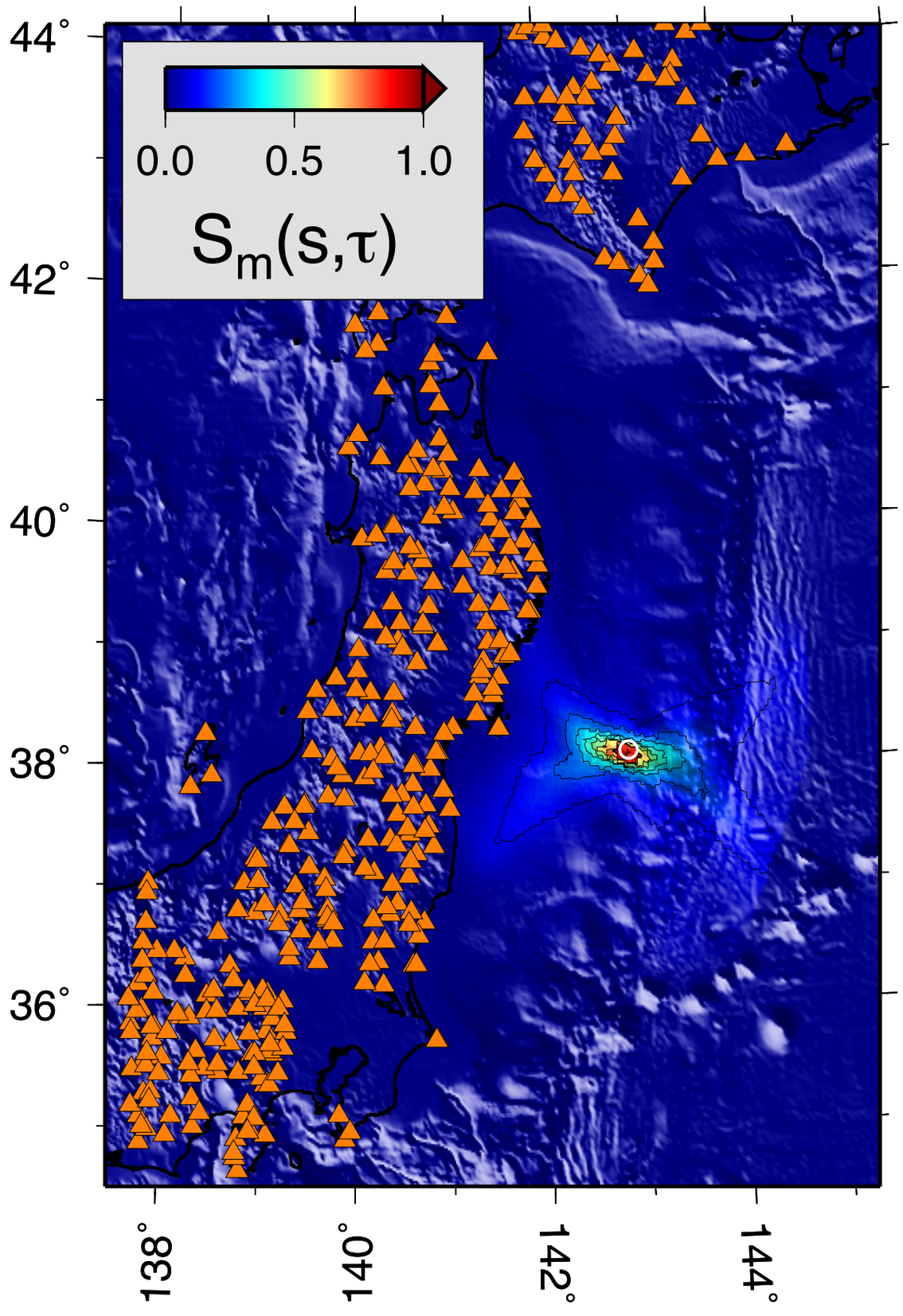

Methods: Data validation

BP of Mw 6.5 aftershock of 28 March using 284 K-NET / KiK-net stations. Same behavior as in synthetic example.

Stack maximum at zero time and true location

Ghost peaks migrate from ESE to WNW

At right: *T*=13s BP result. JMA epicenter is yellow star.

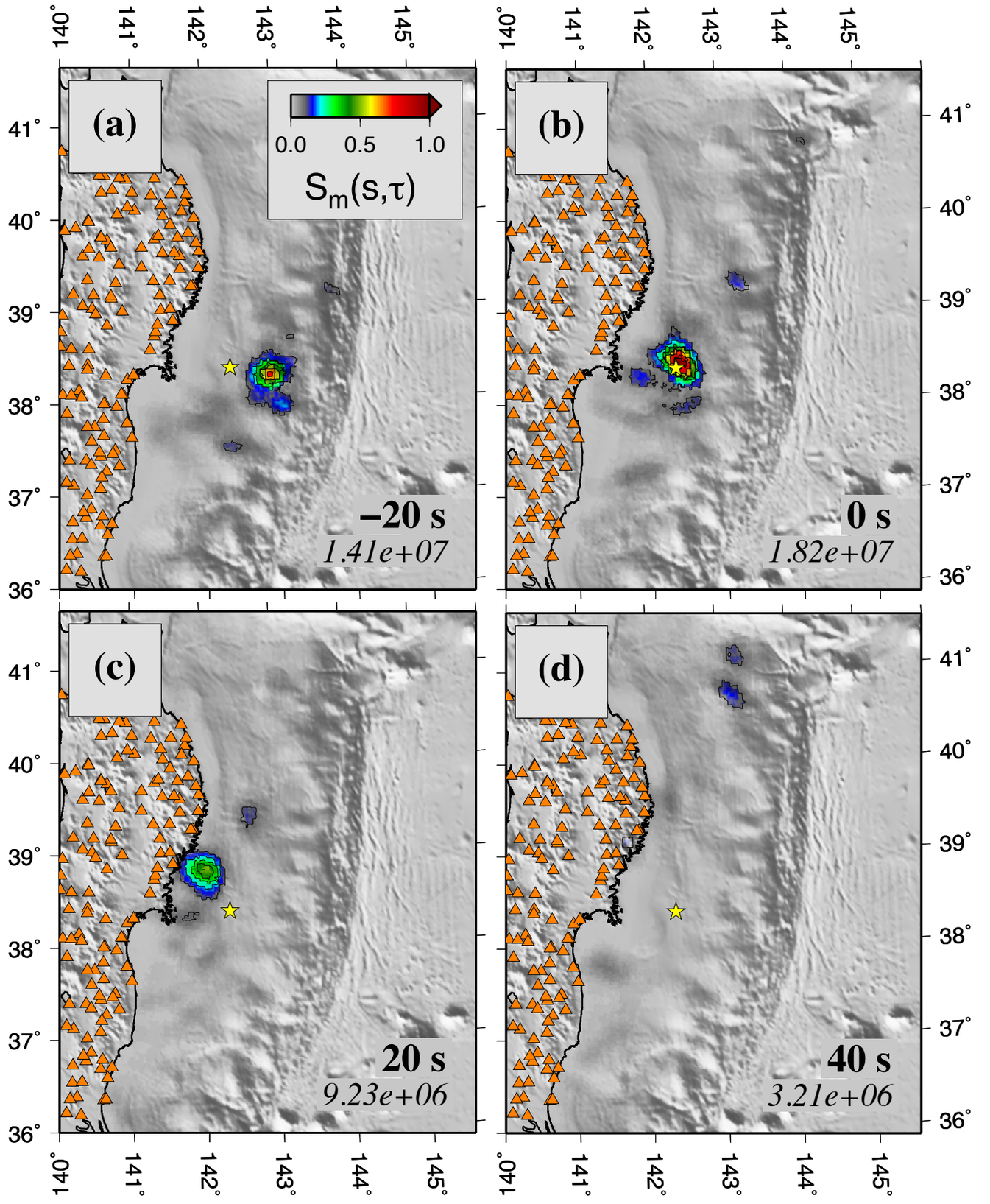

Application to the M_w 9.1 mainshock

Authors performed Rayleigh-wave BP at 13, 20, 30, 50, and 100 s

Prefer a three-stage progressive rupture model

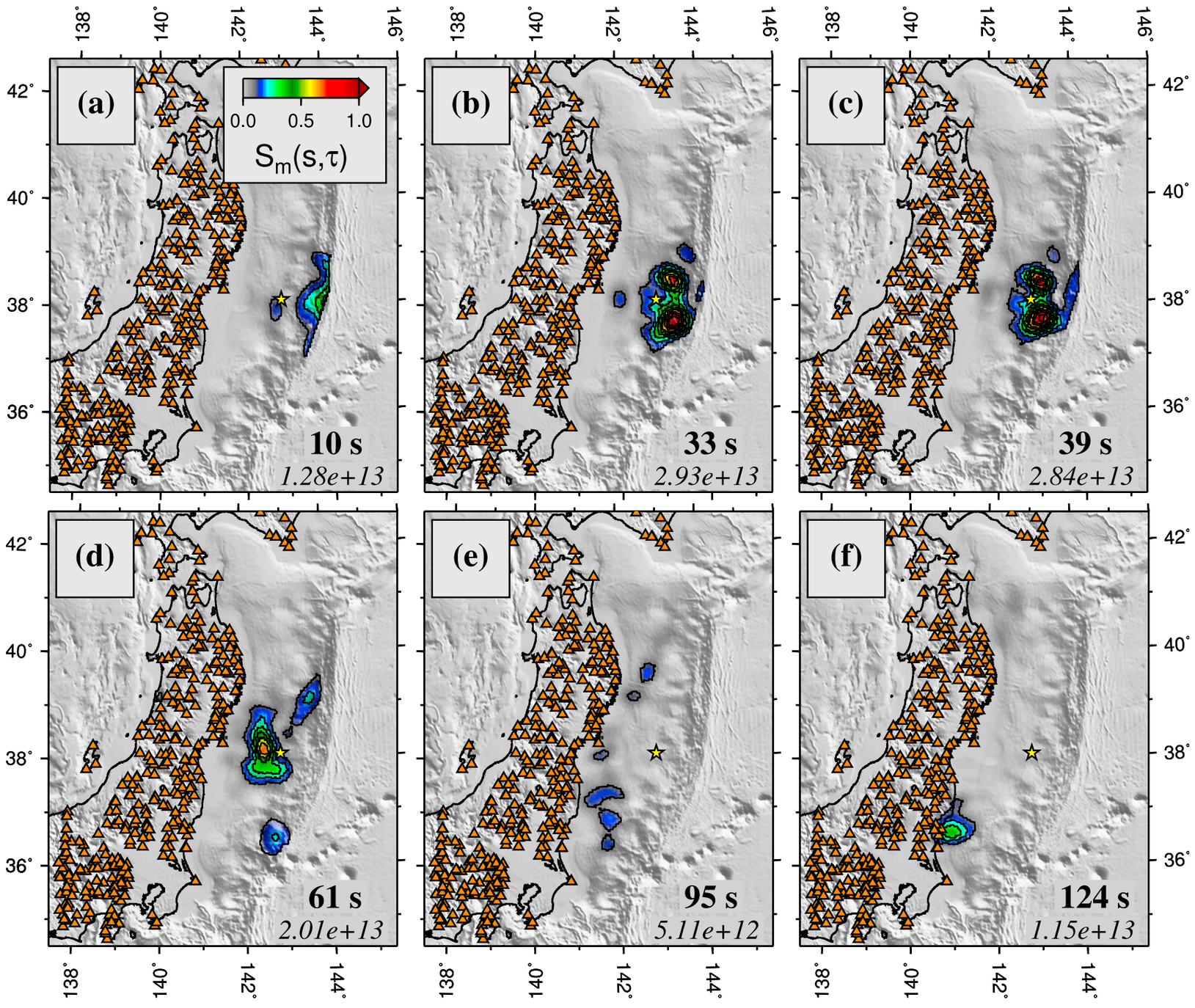

Stage 1: Local maximum in stack amplitude at 10 s just SW of JMA epicenter

At left: 20 s mainshock BP

Application to the M_w 9.1 mainshock

Authors performed Rayleigh-wave BP at 13, 20, 30, 50, and 100 s

Prefer a three-stage progressive rupture model

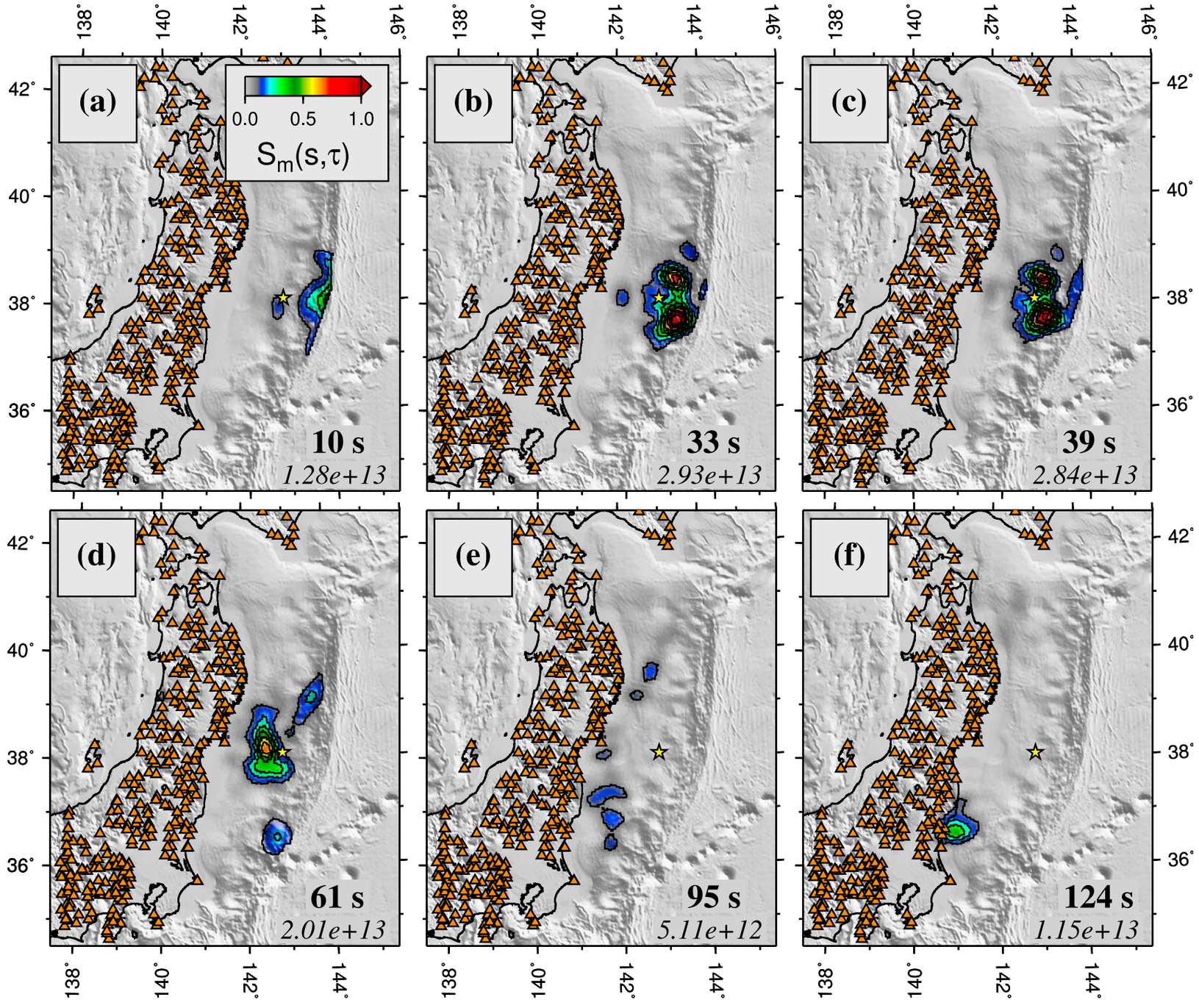

Stage 1: Local maximum in stack amplitude at 10 s just SW of JMA epicenter

Stage 2: Dual peaks to SE (33 s) and NE (39 s)

At left: 20 s mainshock BP

Application to the M_w 9.1 mainshock

Authors performed Rayleigh-wave BP at 13, 20, 30, 50, and 100 s

Prefer a three-stage progressive rupture model

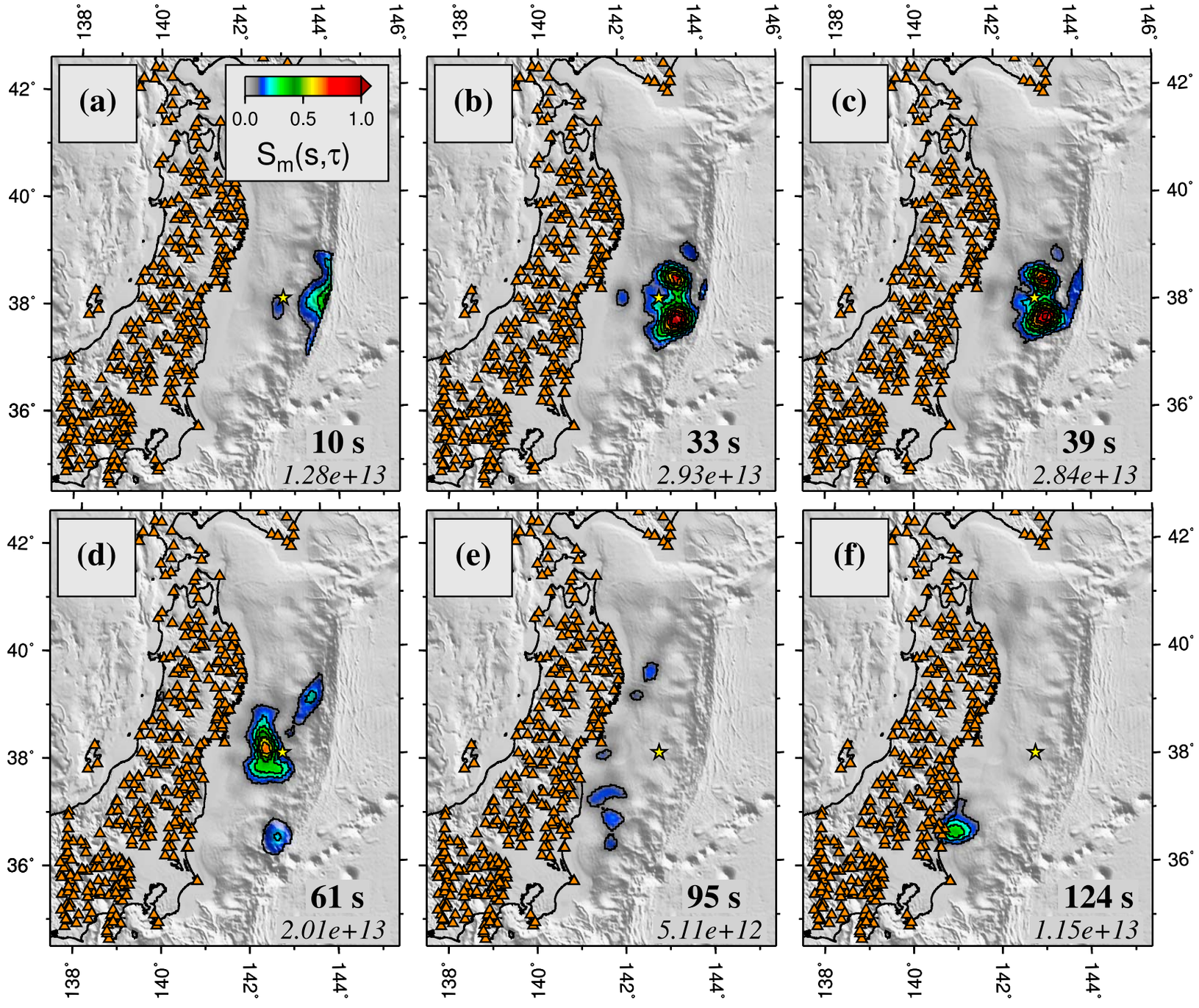

Stage 1: Local maximum in stack amplitude at 10 s just SW of JMA epicenter

Stage 2: Dual peaks to SE (33 s) and NE (39 s)

Stage 3: Northern segment peaks off Iwate at 61 s; Southern segment peaks at 124 s off near Fukushima-oki

At left: 20 s mainshock BP

Application to the M_w 9.1 mainshock

Authors performed Rayleigh-wave BP at 13, 20, 30, 50, and 100 s

Prefer a three-stage progressive rupture model

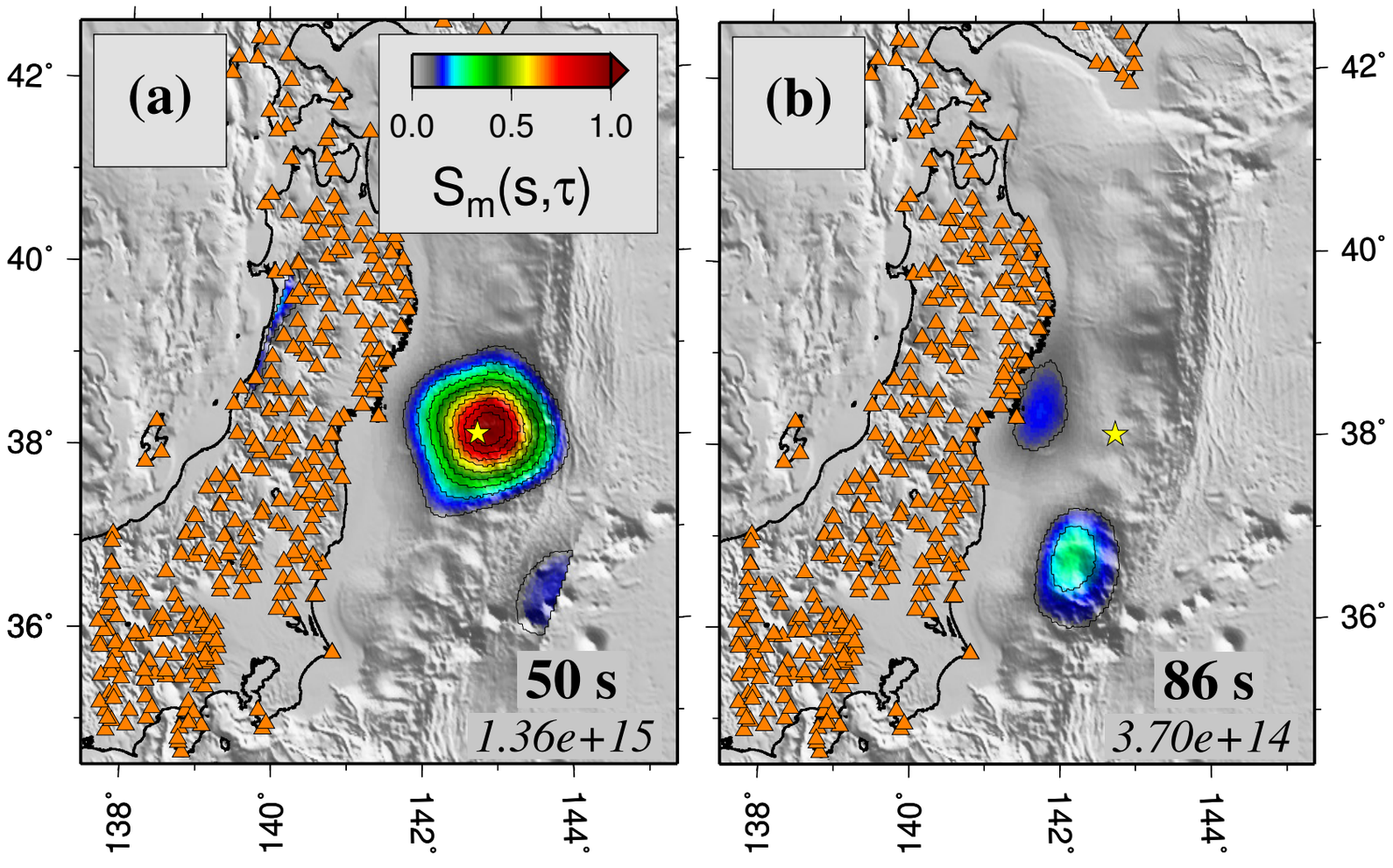

Note difference in timing and distribution

Stage 1: Local maximum in stack amplitude at 10 s just SW of JMA epicenter

At left: 50 s mainshock BP

Application to the M_w 9.1 mainshock

Authors performed Rayleigh-wave BP at 13, 20, 30, 50, and 100 s

Prefer a three-stage progressive rupture model

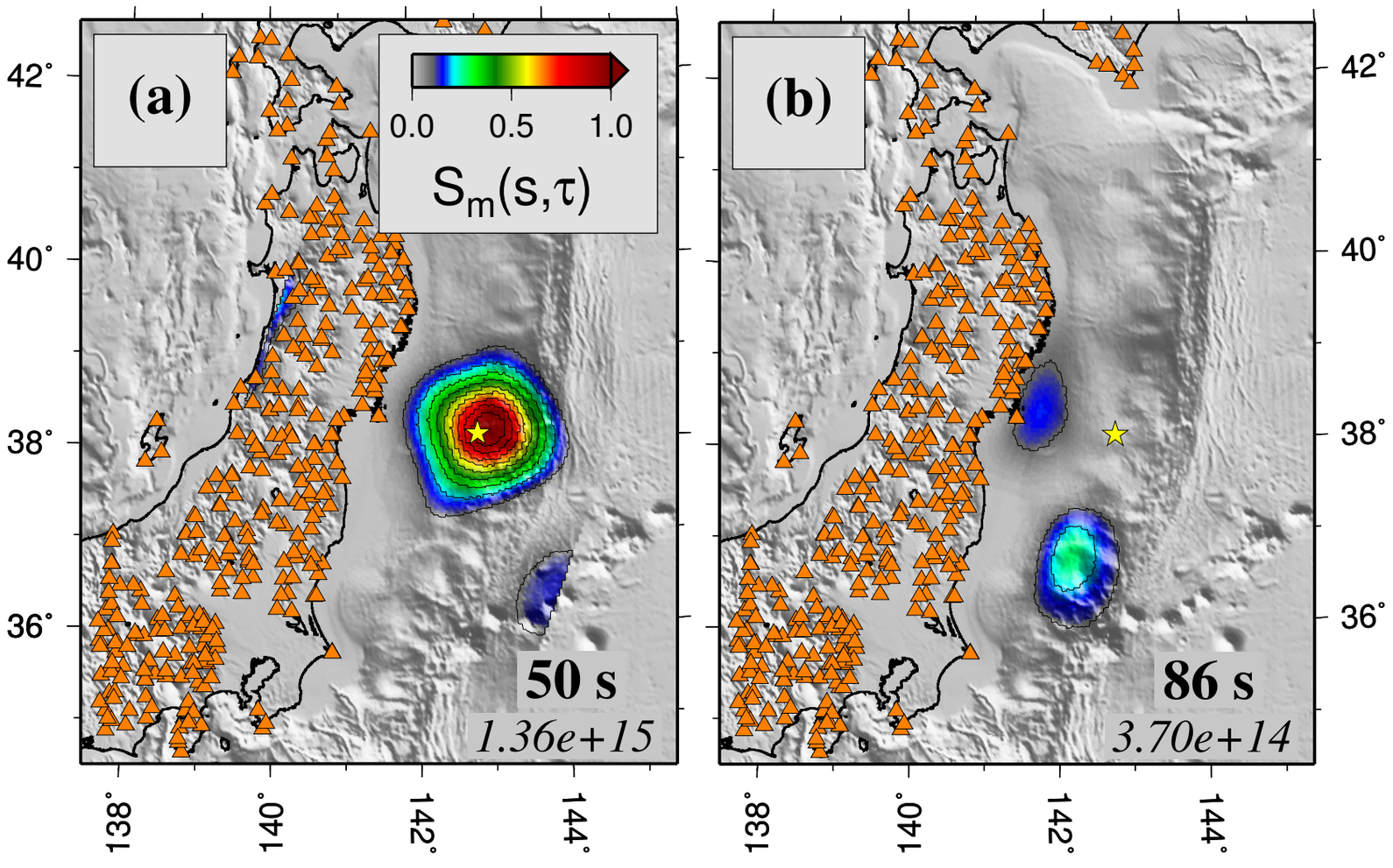

Note difference in timing and distribution

Stage 1: Local maximum in stack amplitude at 10 s just SW of JMA epicenter

Stage 2: Dual peaks to SE (33 s) and NE (39 s)

At left: 50 s mainshock BP

Application to the M_w 9.1 mainshock

Authors performed Rayleigh-wave BP at 13, 20, 30, 50, and 100 s

Prefer a three-stage progressive rupture model

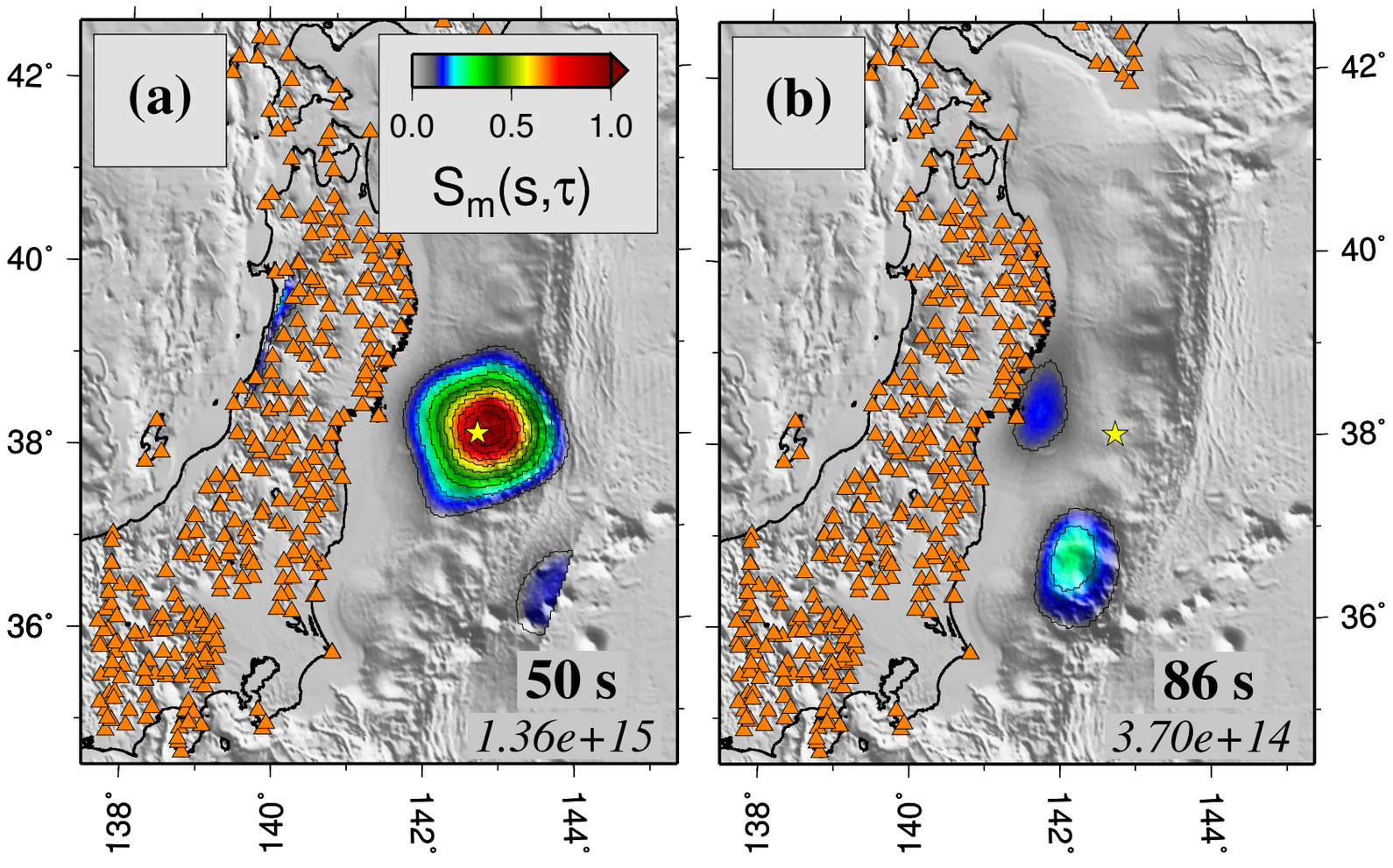

Note difference in timing and distribution

Stage 1: Local maximum in stack amplitude at 10 s just SW of JMA epicenter

Stage 2: Dual peaks to SE (33 s) and NE (39 s)

Stage 3: Northern segment peaks off Iwate at 61 s; Southern segment peaks at 124 s off near Fukushima-oki

At left: 50 s mainshock BP

Application to the M_w 9.1 mainshock

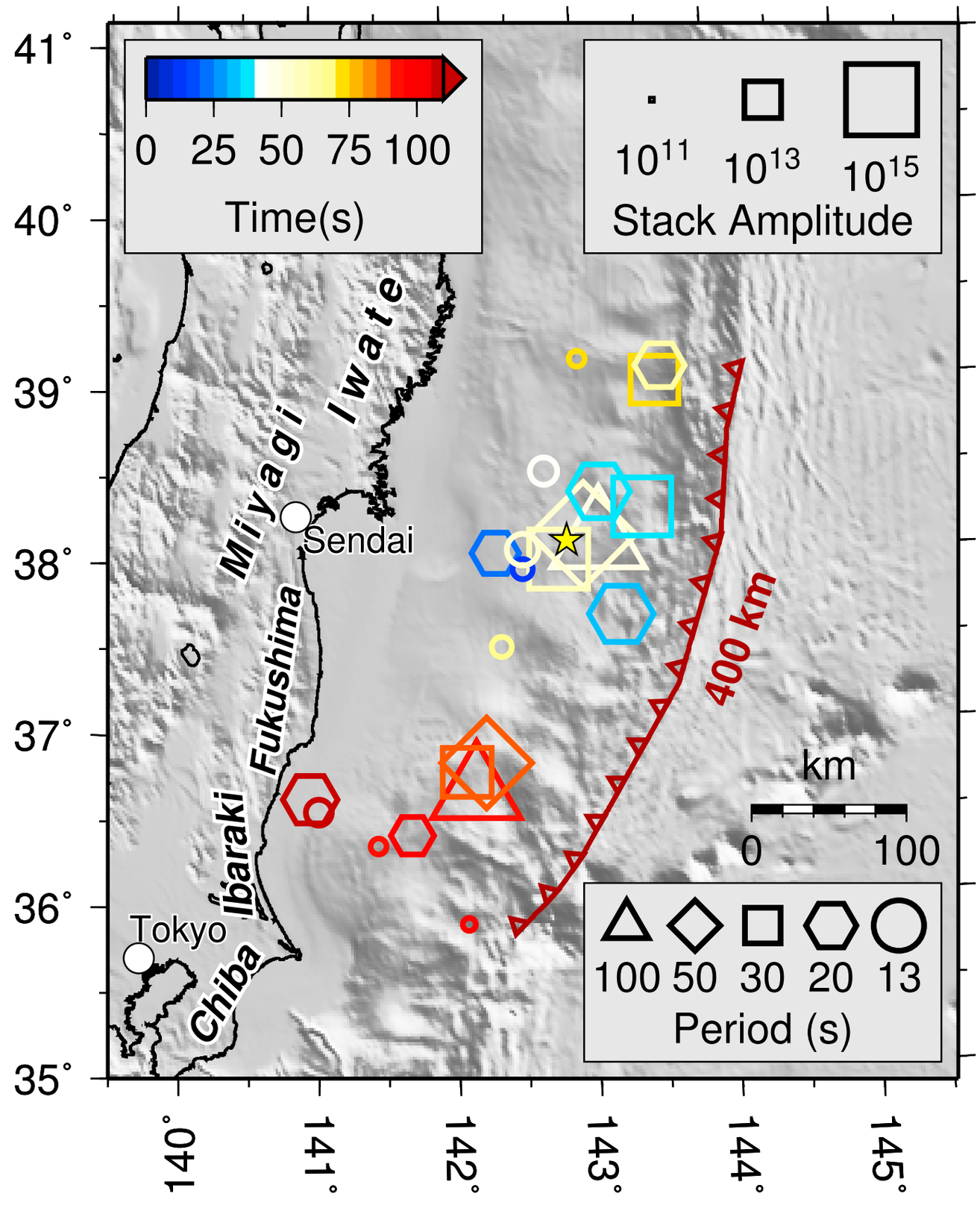

Authors select maxima of coherent ESE-WNW migrating peaks

Stage 2 represents single broad peak at *T*=50,100s; at *T*=30s and shorter, two peaks are observed

Stage 3 northern segment visible *only* at *T*=30s and shorter

Stage 3 southern segment visible at all periods; *single emitter* at *T*=30-100s while *second down-dip* emitter observed at *T*=13,20s

Application to the M_w 9.1 mainshock

Result: coarse, frequency-dependent view of rupture process

Stage 1: rupture down-dip at 2-3.5 km/s; potential up-dip component leading to Stage 2 at ~35 s;

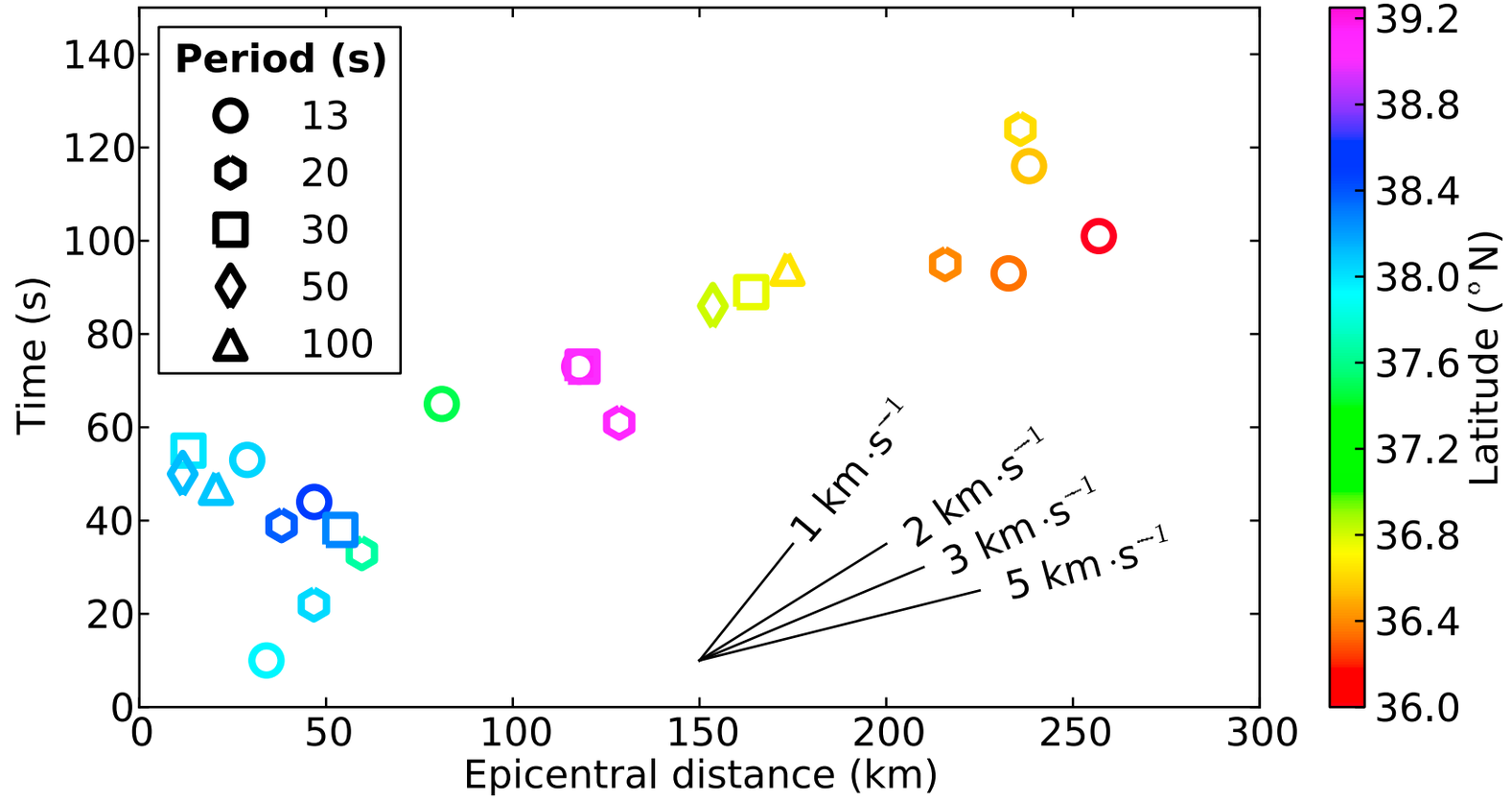

Application to the M_w 9.1 mainshock

Result: coarse, frequency-dependent view of rupture process

Stage 1: rupture down-dip at 2-3.5 km/s; potential up-dip component leading to Stage 2 at ~35 s;

Stage 2: long-period surface waves show onset within 50-100 km of trench near Miyagi-oki (dual-peaked); propagates down-dip, peaking at 40-60 s (strongest maxima over entire rupture);

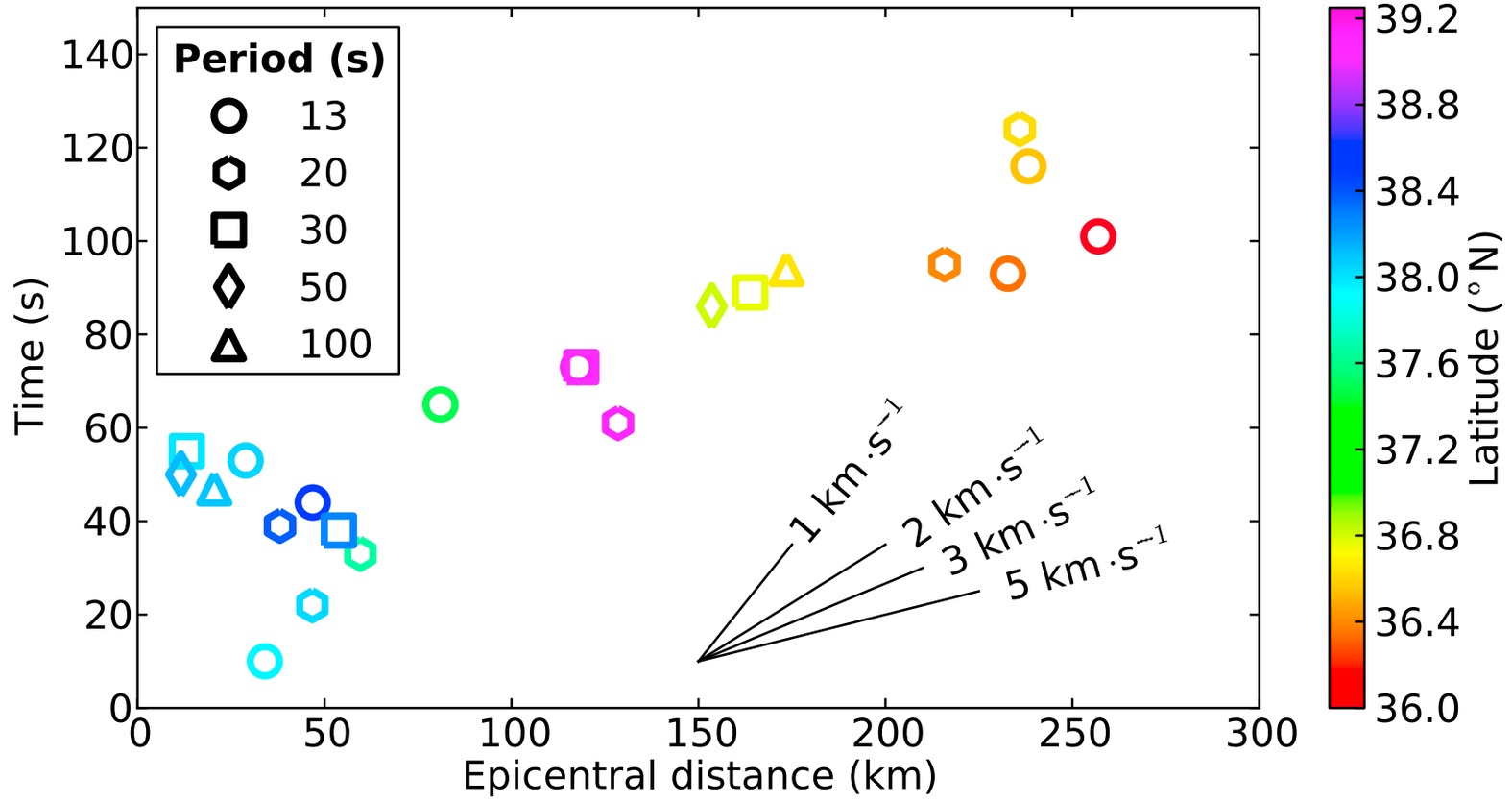

Application to the M_w 9.1 mainshock

Result: coarse, frequency-dependent view of rupture process

Stage 1: rupture down-dip at 2-3.5 km/s; potential up-dip component leading to Stage 2 at ~35 s;

Stage 2: long-period surface waves show onset within 50-100 km of trench near Miyagi-oki (dual-peaked); propagates down-dip, peaking at 40-60 s (strongest maxima over entire rupture);

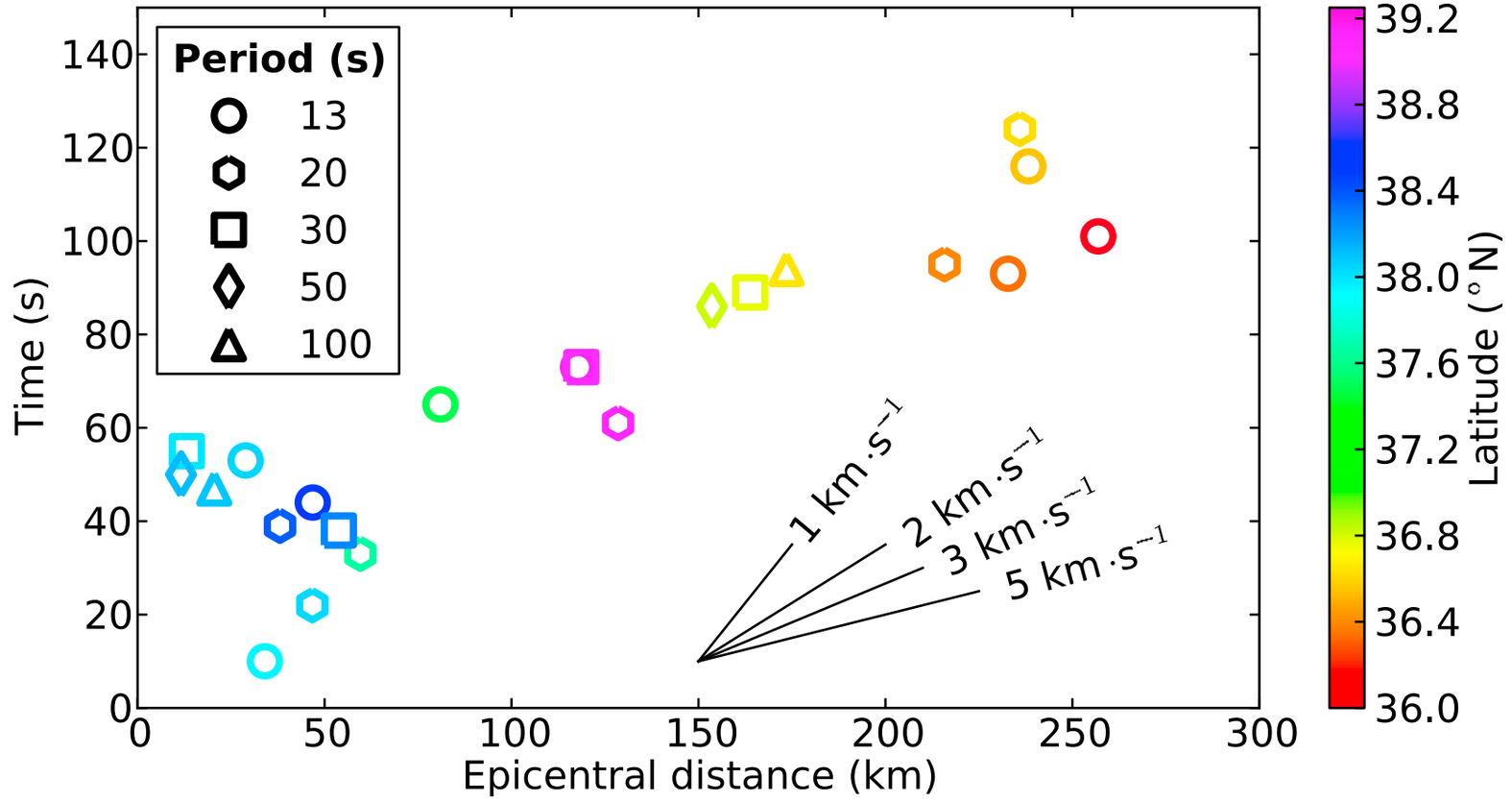

Stage 3: *bilateral* - propagation to north off Iwate at ~60 s (short period: *T*<=30s) and south off Fukushima-oki at 85-100 s. Inferred rupture velocity of 3-3.5 km/s; down-dip component at short periods (T<=20s) below Fukushima-oki at ~120 s

Application to the M_w 9.1 mainshock

Result: coarse, frequency-dependent view of rupture process

Stage 1: rupture down-dip at 2-3.5 km/s; potential up-dip component leading to Stage 2 at ~35 s;

Stage 2: long-period surface waves show onset within 50-100 km of trench near Miyagi-oki (dual-peaked); propagates down-dip, peaking at 40-60 s (strongest maxima over entire rupture);

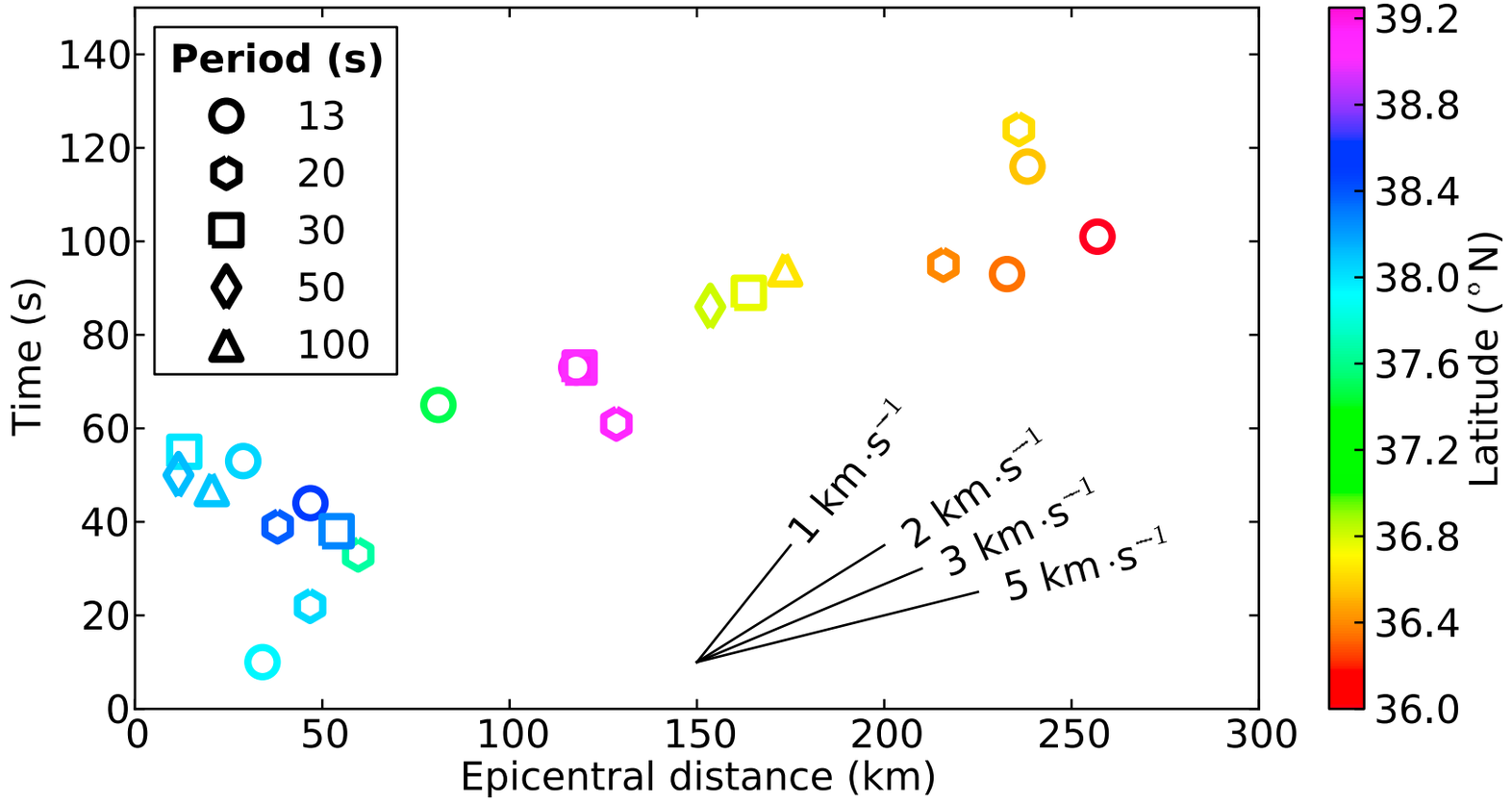

Stage 3: *bilateral* - propagation to north off Iwate at ~60 s (short period: *T*<=30s) and south off Fukushima-oki at 85-100 s. Inferred rupture velocity of 3-3.5 km/s; down-dip component at short periods (T<=20s) below Fukushima-oki at ~120 s

Total rupture along trench > 400km

Comparison with other studies

- Distribution of rupture broadly consistent with finite source models in other studies - particularly maximum slip near epicenter [e.g. Simons et al., 2011]
- Progression (three-stage: 1. weak; 2. strong; 3. bilateral rupture) also broadly consistent with others [e.g. Koketsu et al., 2011]
- Peak moment release in most studies at 60-80 s, while maximum BP amplitudes at 33-55 s (freq. dependent)
- Stage 3 bilateral rupture velocities faster than reported elsewhere: 3-3.5 km/s vs. 2.5 km/s [e.g. Koketsu et al., 2011]
- Stage 3 southern segment stronger than implied by long-period finite fault inversions - source directivity effect on BP? (synthetic experiment suggest this is possible)

Majority of long-period emitters within 100 km of trench, unlike shorter-period BP studies - highlights frequency-dependent radiation effect [e.g. Koper et al., 2011]

Conclusions

- Provides novel method for studying megathrust earthquake rupture
- Inferred distribution of rupture consistent with other studies using a variety of methods (GPS, waveform, tsunami)
- Highlights effect of frequency-dependent seismic wave radiation
- Slip inferred near trench more consistent with studies including longer-period seismic and tsunami waveforms
- Method is low-resolution and limited by the azimuthal coverage of the array, but potentially valuable as it is inexpensive